Published in final edited form as:
Glia. 2010 January 15; 58(2): . doi:10.1002/glia.20918.

Different Astroglia Permissivity Controls the Migration of Olfactory Bulb Interneuron Precursors

Jorge García-Marqués[1], **Juan A. De Carlos**[1], **Charles A. Greer**[2,3], and **Laura López-Mascaraque**[1,*]

[1]Instituto Cajal, CSIC, Av. Dr. Arce, 37, 28002, Madrid, Spain

[2]Department of Neurosurgery, Yale University School of Medicine, New Haven, Connecticut

[3]Department of Neurobiology, Yale University School of Medicine, New Haven, Connecticut

Abstract

The rostral migratory stream (RMS) is a well defined migratory pathway for precursors of olfactory bulb (OB) interneurons. Throughout the RMS an intense astroglial matrix surrounds the migratory cells. However, it is not clear to what extent the astroglial matrix participates in migration. Here, we have analyzed the migratory behavior of neuroblasts cultured on monolayers of astrocytes isolated from areas that are permissive (RMS and OB) and nonpermissive (cortex and adjacent cortical areas) to migration. Our results demonstrate robust neuroblast migration when RMS-explants are cultured on OB or RMS-astrocytes, in contrast to their behavior on astroglia derived from nonpermissive areas. These differences, mediated by astrocyte-derived nonsoluble factors, are related to the overexpression of extracellular matrix and cell adhesion molecules, as revealed by real-time qRT-PCR. Our results show that astroglia heterogeneity could play a significant role in migration within the RMS and in cell detachment in the OB.

Keywords

neurogenesis; astrocyte cultures; RT-PCR; subventricular zone; heterogeneity

INTRODUCTION

Neuroblasts migrating tangentially through the rostral migratory stream (RMS) are flanked by astrocytes, which delineate the migratory pathway (Doetsch et al., 1997; Jankovski and Sotelo, 1996; Peretto et al., 1997; Thomas et al., 1996). Although the neuroblast–glia relationship is less evident in the olfactory bulb (OB), similar appositions may extend into the OB where there is a high density of astrocytes (Emsley and Macklis, 2006). Despite this intimate relationship, the role of glial cells in migration remains controversial. Mature astrocytes are not present during the peak of OB interneuron neurogenesis (Law et al., 1999), although radial glia could provide a cellular scaffold for the early RMS (Alves et al., 2002). *In vitro*, glial cells are not required for chain migration (Wichterle et al., 1997), although they release a soluble substance that induces migration (Mason et al. 2001). Moreover, bidirectional communication between astrocytes and neuroblasts may control the

*Correspondence to: Laura López-Mascaraque, Instituto Cajal (CSIC), Av. Dr. Arce, 37 - 28002, Madrid, Spain. mascaraque@cajal.csic.es.

Additional Supporting Information may be found in the online version of this article.

glutamate and GABA levels implicated in subventricular zone (SVZ) and RMS migratory behavior (Bolteus and Bordey, 2004; Platel et al., 2008).

The mechanisms controlling neuroblasts restriction to the RMS are also poorly understood; neuroblasts are restricted to the RMS and do not colonize surrounding brain areas other than in a few injury-related examples (Faiz et al., 2008). Migrating neuroblasts stop at the SVZ/white matter border and turn back into the SVZ, suggesting a boundary between permissive/nonpermissive migratory zones (Suzuki and Goldman, 2003). The expression of extracellular matrix (ECM) molecules could prevent neuroblast migration into contiguous regions (Thomas et al., 1996). Moreover, a physical barrier formed by RMS-astrocytes may delineate the migratory pathway and prevent cell dispersion out of the RMS, although this is not yet established (Alves et al., 2002; Jankovski and Sotelo, 1996; Peretto et al., 1997).

Here, we investigate the influence of astrocytes in preventing neuroblast excursion from the RMS and their invasion into areas adjacent to the migratory pathway. For this purpose, we undertook comparative cellular and molecular analyses of astroglial cells isolated from zones permissive to neuroblast migration (OB and RMS), and a nonpermissive region (cortex). We show significant differences in the morphological and molecular phenotypes of astrocytes derived from permissive and nonpermissive areas. These differences plausibly affect the behavior of migratory neuroblasts and thus shed light on the mechanism(s) regulating the specificity of cell migration within the RMS.

MATERIALS AND METHODS

Animals

C57BL/6 mice aged P1–P3 and P18 (n = 186 and 18, respectively) were used. Animals were either raised at the Cajal Institute or provided by Charles River Laboratories (for the experiments carried-out in Yale University). The handling and sacrificing of the animals used was in accordance with the Spanish (RD1201/2005 and Ley 32/2007) and European Commission guidelines (2003/65/CE). Experimental procedures were approved by the Cajal Institute and the Yale Animal Care and Use Committee. Pups aged P1 to P3 were anesthetized by hypothermia and decapitated, whereas P18 mice were sacrificed with Equithesin (3 mL Kg^{-1} body weight).

Immunostaining

For immunohistochemistry, anaesthetized P2 and P18 mice were perfused transcardially with 4% paraformaldehyde (PF) in PB and the brains post-fixed in PF overnight. Vibratome sections (30 μm) were obtained in sagittal or coronal planes and transferred to 0.2% Triton X-100 (PBS-T). Culture samples were fixed with PF for 15 min and then washed in PBS-T. Sections and cultures were blocked in 2% bovine serum albumin (Sigma) for 45 min, and then incubated overnight in the primary antibody. After rinsing samples were incubated with secondary antibodies for 90 min and then counterstained with Hoechst (10 μg mL^{-1}, Sigma).

Sections and cultures were immunostained with the following: anti-Doublecortin (DCX, 1:2,000; Chemicon); anti-glial-fibrillary-acid-protein (GFAP, 1:500; Dako); and Anti-β-Tubulin (TuJ1, 1:1,000; gift from Dr. Frankfurter). To visualize the antibodies different secondary antibodies were used: biotinylated-Goat-anti-Guinea-Pig (Atom Vector, 1:200); Alexa 568 and 488 (Molecular Probes, 1:2,000). Biotinylated antibodies were revealed using Alexa 488 Streptavidin (Molecular Probes, 1:2,000). For all antibodies, control samples were stained omitting the primary antibody and no staining was seen.

Astrocyte Monolayer Cultures

Purified astrocyte monolayers were generated following the modified protocol of Banker and Goslin (1991). Postnatal mice (P1–3) were decapitated and brains were removed and placed in cold HBSS (GIBCO). Brains were embedded in 3% low-melting-point agarose, (Pronadisa) diluted in dissecting medium (L15 supplemented with 10% FBS, GIBCO) at 43°C. After cooling, embedded brain was vibratome sectioned (200 μm), and dissected (Fig. 1A). We selected both OB (Fig. 1A, excluding the subependymal-, glomerular-, and nerve-layers to avoid contamination with ensheathing cells or RMS elements) and RMS (Fig. 1A, RMS, horizontal arm excluding the OB area) as permissive regions. As nonpermissive regions, the anterior frontal cortex (Fig. 1A, Cx) was chosen, as well as other areas adjacent to the RMS (Fig. 1A, AA). Selected tissues were collected separately in tubes and mechanically dissociated. Cells were resuspended in DMEM/F12 medium (glutamine-free, GIBCO) supplemented with 10% FBS, penicillin/streptomycin (GIBCO), and Glutamax (GIBCO), and then plated in flasks poly-L-lysine-coated (10 μg mL^{-1}, Sigma). Cell cultures were maintained in a 5% CO_2 atmosphere at 37°C, replacing the culture medium twice a week.

After 12–15 days *in vitro* (DIV), purified astrocytes were obtained by shaking flasks at 280 rpm o/n at 37°C. Attached cells were trypsinized (trypsin-EDTA; GIBCO) and seeded onto poly-L-lysine-coated-plates (10 μg mL^{-1}), at the same cell density depending on the experiment (see below).

Contact Co-Cultures of RMS-Explants on Astrocyte Monolayers

The same number of astrocytes from each source (4–6 × 10^4 cells/well) was plated in 48-well plates and grown to confluence (2–7 days). Before explant addition, plates were shaken again to remove cells other than astrocytes. RMS-explants (P1–P3) were then placed in each well and co-cultured for 1 DIV.

Complementary experiments were performed to examine the response of RMS-explants in the presence of two different astrocyte monolayers in the same dish. Astrocytes from different origins were separately plated in parallel in the same well, as described below. Plates were prepared by dividing the dish with a strip of parafilm® (~200-μm wide), applied by pressure, after which the plates were sterilized and then poly-L-lysine coated (Rydholm et al., 2005). Two drops (15 μL) containing 15,000 astrocytes from two different origins were plated on each side of the parafilm strip that was removed after reaching confluence. Two RMS-explants were placed on each monolayer, while in other experiments only one explant was plated between both astrocyte monolayers. Co-cultures were maintained for 1 DIV as described above.

Contact-Free Co-Culture of RMS-Explants and Astrocyte Monolayers

To test for diffusible factors, RMS-explants were plated on coverslips covered with collagen and suspended above the astrocyte monolayer by three paraffin pillars (modified from Banker and Goslin, 1991). RMS-explants obtained as above were embedded in three-dimensional collagen matrices prepared from 10 μL of Type-I-collagen (BD Biosciences). After gelling, coverslips were inverted and fixed to the astrocyte monolayer, which prevented direct physical contact but allowed these cell types to share the culture medium (400 μL of culture medium). The cultures were incubated for 3 days as described above.

Dynamic Analysis of Migration by Video Time-Lapse Recording

The dynamic nature of neuroblast migration was analyzed in contact co-cultures on the different astrocyte monolayers. Video recording of cell migration started either 6 h before fixation, or immediately after plating. Images were acquired with a 10× objective at 3-min

intervals for 6 h in at least four different explant positions. In some cases, explants were recorded during the first 18 h at 5-min intervals. Time-lapse video images were acquired with an inverted microscope (Leica, DMI6000B) equipped with a CO_2 incubation system (Leica BL).

Quantitative RT-PCR Analysis of Differential Gene Expression

Total RNA was extracted from confluent astrocyte cultures and real-time RT-PCR was performed to assay the expression of genes encoding ECM and cell adhesion molecules (PAMM-013; Superarray). Astrocyte cultures were shaken and replated, and the total RNA was extracted using the RNEasy kit (Qiagen). RNA from different astrocyte sources (500 ng) was used to generate cDNAs, and signals from genomic DNA and impurities that might affect the RT-PCR assay were ruled out by quality control real-time RT-PCR-array (PAMM-999; Superarray). Fluorescent emission was recorded in real-time (Chromo-4-Four-Color Real-Time-PCR-Detector; MJ Research). All the above procedures were carried out according to the manufacturer instructions.

For tissue samples, RNA from OB-, RMS-, and Cx-areas were extracted from P2 mice as above and real time RT-PCR was used to test for the expression of following genes (Power SYBR Green RNA-to-CT 1-Step Kit, Applied Biosystems): Thbs-1 (PrimerBank ID: 7110725a1), Sparc (6678077a1), Ecm1 (4103926a1), Cttna1 (6753294a1), Lama3 (1922889a1), Cdh2 (6680 902a1). All of these primer sequences were obtained from PrimerBank (Wang and Seed, 2003). Data were normalized to 18S-ribosomal-RNA (sense-CGGCTACCA CATCCAAGG, antisense-GCTGCTGGCACCAGACTT).

Data Analysis

Significant differences between three or more groups were evaluated using ANOVA followed by Bonferroni analysis. Student *t* test (two-tailed) was used to compare two groups and a linear regression analysis to evaluate relationships between parameters. Results were confirmed in at least three independent experiments. Statistical significance was considered with a *P*-value of $P < 0.05$ and all statistical analyses were performed using GraphPad Prism 5.0.

Migration areas were measured using the Area-Calculator-ImageJ-plugin (NIH), and the time-lapse images to track individual cells. Only cells whose trajectory was identifiable were analyzed (by maximum proximity to random coordinates). Cell tracking was performed using the Manual-Tracking-ImageJ-plugin (Institut Curie, France). The following indices and values were defined for analysis: (a) Migration index (M.I.), total area divided by the explant area; (b) Maximum net displacement, maximum distance covered by each cell relative to the origin of migration; (c) Trajectory, total length traveled from the origin of migration to the final position; and (d) Winding index, trajectory divided by maximum net displacement.

Fluorescent images (Leica, DMI6000B; Nikon, Eclipse E600) were captured using a digital camera (Leica DFC350 Fx; Nikon, DXM 1200F). Confocal images were acquired with a Leica TCS-SP5 microscope. Images were adjusted for brightness and contrast with Adobe Photoshop CS3 (v.10.0). For time-lapse microscopy, phase contrast images were captured with a CCD camera (Leica DFC350 Fx). Movies were mounted using LAS AF version: 1.5.1 software (Leica).

RESULTS

The Astrocyte Source Determines Their Influence on RMS Neuroblast Migration

To analyze the influence of astrocytes on RMS neuroblast migration, we cultured RMS-explants on astrocyte monolayers generated from different areas (Fig. 1A). We selected P1–P3 mice because, although the glial population is not fully mature, it corresponds to the peak of postnatal neurogenesis.

For this study we defined areas as permissive for migration (RMS and OB), or nonpermissive (Cx and AA). As a nonpermissive area we chose the cortex because migration from the SVZ into Cx rarely, if ever, occurs other than in some injury models. We first confirmed the GFAP-positive cells in the OB, RMS and Cx (Fig. 1B–D, respectively). Then, we performed dual immunostaining (Fig. 1E–G) to define the neurons migrating from the explant (TuJ1, green) on the different monolayers (GFAP, red). Explant cell migration was analyzed by calculating the migration index (M.I., Fig. 1H). The highest M.I. (12.44 ± 1.26, mean ± SEM) from RMS-explants was on a monolayer of OB-derived-astrocytes (Fig. 1E,H), while the M.I. was lower for RMS-derived-astrocytes monolayer (7.47 ± 0.23, Fig. 1F,H). However, the M.I. was significantly lower when RMS-explants were cultured on nonpermissive areas (4.27 ± 0.32, Fig. 1G,H). To test whether cortical-derived-astrocytes were nonpermissive in the culture conditions, or astroglia from other nonpermissive areas *in vivo* also retained this characteristic *in vitro*, we repeated this assay using AA-derived-astroglia (Fig. 1A,AA). Again, the M.I. of RMS-explants plated on AA-astrocyte-monolayers was significantly lower (3.86 ± 0.33) than on OB- and RMS-derived-astrocytes (Fig. 1H).

We next asked whether differences in the proportion of astrocytes were responsible for the differences in migration. However, the astrocyte monolayers were over 91–92% GFAP-positive (Fig. 1I). Thus, no significant differences between the astroglial sources were found ($P = 0.529$). These data indicate that cell migration differences between RMS over RMS-, OB-, and Cx-derived-astrocyte monolayers were not due to the proportion of astrocytes in the cultures. Since differences in proliferation might affect the cell density until confluence was reached, we studied whether the M.I. was related to the density of the astrocyte monolayers. Linear correlation analyses were performed between culture cell density and the M.I. for each well, revealing that differences in cell density did not account for the different M.I. (Fig. 1J, $P = 0.501$).

Heterogeneity in Astrocyte Morphology

GFAP-positive astrocytes isolated from different regions displayed distinct morphologies. Astrocytes from both OB (Fig. 2A,B) and RMS (Fig. 2C,D) were elongated with a fusiform morphology (Fig. 2B,D). This bipolar morphology was more common and evident in RMS-derived-astrocyte monolayers, whereas in OB-derived-astrocytes the elongated morphology coexisted with other more flattened cells. However, both OB- and RMS-derived-monolayers were clearly distinct from Cx-derived-monolayers which rarely included elongated astrocytes (Fig. 2E,F). Rather, monolayers from Cx-derived-astrocytes exhibited a flattened star-like and bushy morphology, with many fine terminal processes protruding from the main cellular processes (Fig. 2F). This heterogeneity reflects intrinsic differences in the morphological response with respect to similar *in vitro* conditions.

Nonsoluble Factors from Astrocytes Mediate the Migration Index Differences

To determine whether surface bound or soluble molecules mediated the significant M.I. differences, we performed two additional assays. First, the M.I. was measured when two RMS-explants were plated on two different monolayers within the same culture dish (Fig.

3A) separated by a band without cells (Fig. 3B). In this assay, the M.I. differed on the alternative substrates, despite their presence in the same culture well. The relationship between the M.I. from both explants in the same well was defined as the side ratio (Fig. 3C). When OB-astrocytes were opposite cortical-astrocytes, the side ratio evidenced a higher M.I. for OB, than Cx-derived-astrocytes (side ratio mean ± SEM; 4.63 ± 0.55). Similarly, when OB-derived-astrocytes were opposite those from the RMS the M.I. was higher for OB (2.31 ± 0.21). Finally, RMS-derived-astrocytes promoted a higher migration than Cx-derived-astrocytes (1.71 ± 0.09). In all cases the side ratios were greater than 1.0, indicating that any soluble factors released into the culture medium did not contribute significantly to migration. This relationship was maintained when only one RMS-explant was placed with a choice of two alternative astrocyte monolayers in the same culture well (Fig. 3D,E). The striking asymmetric migration onto the RMS-substrate rather than the Cx-substrate (Fig. 3D) was not evident with RMS-explants on paired Cx-monolayers (Fig. 3E).

To further test whether soluble factors affect migration, the RMS-explants were isolated from the underlying astrocyte monolayers. The explants were plated on a plastic coverslip embedded in a three-dimensional collagen matrix and suspended above the astrocyte monolayers by three pillars that prevented the collagen matrix, containing the explant, from making direct contact with the monolayer (Fig. 3F). After 3 DIV, the explants were immunostained for TuJ1 (Fig. 3G). Under these conditions, there were no significant differences in the migration between OB-, RMS-, and Cx-derived astrocyte monolayers (Fig. 3H), even when compared with cultures without monolayers ($P = 0.309$). Thus, contact mediated factors exert a more decisive influence on the migration differences than soluble cues produced by the astrocyte monolayers.

Dynamics of Neuroblast Migration: Time-Lapse Video Microscopy Study

To explore the dynamic temporal and cytological aspects of the differences in M.I., we analyzed the behavior of RMS neurons using time-lapse video-microscopy. We compared the migratory behavior of cells from RMS-explants cultured on OB-, RMS- or Cx-derived-astrocyte monolayers, capturing frames at 3-min intervals and tracking individual cells for the last 6 h in the culture. Under these conditions, differences in the migration of neuroblasts on the three substrates were immediately apparent, even a short time after plating the RMS-explant on the different monolayers (Fig. 4A–C; Supp. Info. Movies 1–3). After tracking 30 cells, their trajectories were plotted from the origin point (Fig. 4D–F; Supp. Info. Movies 4–6); these trajectories occupied areas consistent with our previous results (Fig. 4D–F).

We compared the average speed of RMS cells in the final 6 h of a 24-h culture period and RMS neuroblasts migrated faster on OB- than on Cx-derived-astrocytes (mean ± SEM; OB = 72.4 ± 2.93 μm h^{-1}; Cx = 57.47 ± 3.09 μm h^{-1}; $P < 0.05$). No significant differences were observed in migration speed on the OB- and RMS-derived-astrocytes (64.40 ± 3.7 μm h^{-1}) or RMS-and Cx-derived substrates. We then quantified the maximum net displacement during the 6-h period (Fig. 4H), although no significant differences were observed for this value on the different astrocyte substrates ($P = 0.06$). Since cell migration is interrupted by periods of no movement (Bovetti et al., 2007a; Wichterle et al., 1997), we analyzed the pauses in cell migration relative to the migratory substrate (Fig. 4I). RMS neuroblasts paused for significantly longer periods of time on Cx- than on OB-derived-astrocytes ($P < 0.01$).

To compare the trajectories from RMS-explants on the different monolayers, we analyzed the ratio between the trajectory and the net displacement, defined as the “winding index” (Fig. 4J). Cells with a lower “winding index” migrated in a straight path from the start to the end point, while those with a higher index followed a more tortuous route. However, there

were no significant differences in this index between the RMS cells cultured on the different monolayers ($P = 0.821$).

To explore the mechanisms underlying the migratory behavior of these cells along the time course, we next analyzed the dynamics of different parameters during 6-h sequences. We determined the distance traveled by neuroblasts in each 3-min interval (referred to as a step) and represented in a histogram as percentage step distance (Fig. 4K). The most repetitive distance interval was 2 μm for all astrocyte sources. However, in relation to the staccato migratory behavior described for RMS neuroblasts, the number of cell pauses (defined as distances less than 1 μm) occupied an important step percentage. We found that RMS cells co-cultured on Cx-derived-astrocytes had the highest percentage of pauses, represented as a 0 value in the step length axis (Fig. 4K). These results were consistent with the preceding analyses in which such pauses were also more frequent on Cx-derived-astrocytes.

We then analyzed the average distance traveled by cells from the point of origin in relation to time. Cell dynamic curves on the different monolayers show that, while the average distance increased linearly on OB-, RMS- and Cx-derived-astrocytes, the distance traveled by RMS cells saturated ~200 min from the start point (Fig. 4L). This correlates with the increase in the number of paused cells in relation to the culture time on both RMS- and Cx-derived-astrocytes ($P < 0.0001$), but not for explants on OB-derived-astrocytes ($P = 0.424$; Fig. 4M).

In summary, time-lapse experiments revealed many dynamic parameters related to the cell migratory behavior that help to explain the differences in migration on OB- and Cx-derived astroglia seen in the statically analyzed cultures.

Cell Adhesion and ECM Related Gene Expression

Because the differences in the M.I. appear to be mediated by contact factors, we used real-time RT-PCR to analyze and compare the expression of 84 genes related to cell adhesion and ECM. When we first assessed the differential gene expression patterns in the three astrocyte monolayers (see Table 1 in Supporting Information), many genes were upregulated in OB, compared with Cx-derived-astrocytes (Fig. 5A, 16 upregulated genes vs. 2 downregulated genes). A similar profile was found for RMS, relative to Cx-derived-astrocytes (Fig. 5B, 24 upregulated genes vs. 3 downregulated genes). In contrast, between OB- and RMS-derived-astrocytes we did not find strong differences in gene expression (Fig. 5C, 12 upregulated genes in RMS vs. 6 downregulated genes). Hence, cell adhesion and ECM related gene expression appeared higher in OB and RMS when compared with Cx-derived-astrocytes.

We analyzed further the relative gene expression levels that differed significantly in the different monolayers (Fig. 5D–F and Table 1 in Supporting Information). The differentially expressed genes were ranked and sorted on the basis of their relative expression. The results of the real-time RT-PCR experiments for the genes highly expressed are shown in Fig. 5D (relative expression considered as over 5×10^{-7} for the highest level of expression). Several candidate genes showed large differences in expression, as the *Thbs1* (11.7-fold greater in OB- than in Cx-astrocytes and 6.41-fold greater in RMS-astrocytes), or *Col1a1* (10.1-fold greater in OB-astrocytes relative to Cx-astrocytes). In regard to genes with a comparative relative expression between 5×10^{-7} and 2×10^{-8} (Fig. 5E), the greatest differences were found for the *Ctnna1* gene, which showed six-fold stronger expression in OB and RMS than in Cx-astrocytes (6.38-fold for OB, 6.88-fold for RMS-astrocytes). Also, *ECM1* was more strongly expressed in OB and RMS than in Cx-derived-astrocytes (5.91-fold for OB, 5.8-fold for RMS-astrocytes). It was noteworthy that the highest comparative gene expression in Cx-astrocytes included the more weakly expressed genes (Fig. 5F). For example, *Adamts2*

(-1.71-fold for OB, -1.96-fold for RMS-derived-astrocytes), *Itgam* (−8-fold for RMS-astrocytes) or *Hapln-1* (−13.6-fold for OB-astrocytes) all of which were expressed more weakly in the OB and RMS-astrocytes than in Cx-astrocytes. However, other genes in this category were upregulated in OB- and RMS-derived astroglia when compared with Cx astroglia, such as *Lama3* (7.98-fold for OB- and 6.93-fold for RMS-astrocytes). An important difference was observed for *Col4a3*, which was upregulated 27.8-fold in OB- with respect to Cx-derived-astrocytes. The importance of these data is that the differences in gene expression detected in cultures can be also detected *in vivo*. Therefore, we performed RT-PCR from freshly-dissected P2 brain tissue for some selected genes. As expected, *in vivo* and *in vitro* assays correlate very well for some genes (Fig. 5G), although we also found important differences. Both *in vivo* and *in vitro, Thbs 1* and *Ecm1* are upregulated for OB- and RMS-astrocytes (Fig. 5G) when compared with Cx-derived-astrocytes, while *Ctnna1* and *Lama3* are only upregulated in the RMS-derived-astrocytes (in culture it is also upregulated for OB-derived-astrocytes). In contrast to *in vitro* results, *Sparc* and *Cdh2* are not upregulated *in vivo*, although the expression level between OB and RMS is comparable both *in vivo* and in *vitro*.

In sum, these analyses suggest that gene-specific expression of both cell adhesion and ECM molecules are likely to contribute to the differential effect of OB-, RMS-, and Cx-derived-astrocytes on the migratory behavior of neuroblasts from the RMS.

DISCUSSION

We show that astroglia isolated from regions more or less permissive to neuroblast migration show a significant heterogeneity in their ability to support migration, their morphology, and molecular properties. These results suggest an important role for astroglia in regulating migration of RMS neuroblasts *in vivo*.

Astroglia Heterogeneity Differentially Affects Neuroblast Migration

Our results demonstrate that astrocytes isolated from permissive areas support more extensive migration than those from nonpermissive areas. Throughout life SVZ neuroblasts migrate toward the OB in complex chains ensheathed by astrocytes (Lois et al., 1996; Peretto et al., 1997). Three main lines of evidence suggested that astroglia were not essential for migration: (1) mature astroglia are not present during the early period of neurogenesis (Law et al., 1999); (2) SVZ explants exhibit chain migration in Matrigel in the absence of astroglia (Wichterle et al., 1997); and (3) specialized contacts exist between neuroblasts but not between astrocytes and neuroblasts (Lois and Alvarez-Buylla, 1994). By contrast we show here, together with previous results (Alves et al., 2002; Pencea and Luskin, 2003), that GFAP is expressed in the SVZ/RMS by the first postnatal week, suggesting that astrocyte progenitors could substitute for the absence of mature astrocytes (Alves et al., 2002). In addition, although chain migration can occur in the absence of astroglia, Matrigel is a mixture of ECM components secreted by EHS tumors (Kleinman and Martin, 2005) that may substitute for glial-derived factors. Thus, although there is no evidence for specialized contacts within the RMS, astrocytes may regulate cell migration directly as a cellular scaffold, or, by providing a molecular scaffold similar to artificial substrates *in vitro*. Consistent with this hypothesis (see Fig. 5G), ECM proteins are abundant in RMS (Thomas et al., 1996) as well as in OB, where an ECM layer appears to be interposed between astrocytes and neuroblasts (Bovetti et al., 2007b).

Consistent with the new data we present here, additional lines of evidence support the notion that astrocytes may be a pivotal determinant of RMS neuroblast migration. For example, neuroblast migration is 20% faster in chains within glial tubes than in glial-free environments (Bovetti et al., 2007a). Similarly, it is slower in nonglial ensheathed

parenchymal chains (Luzzati et al., 2003). Moreover, astrocytes enhance migration by regulating extracellular GABA (Bolteus and Bordey, 2004) and releasing a soluble protein (Mason et al., 2001). Finally, astroglial tunnels may constitute a physical barrier that defines boundaries preventing the exit of migrating cells (Alves et al., 2002; Jankovski and Sotelo, 1996).

The role of glia in patterning and boundary establishment is known elsewhere in the CNS. Thus, radial glia delimits migratory neuronal fate with regard to process orientation (Noctor et al., 2001). Similarly, differences in permissiveness of medial- and lateral-glia promote a barrier for axonal growth across the mid-brain midline (Garcia-Abreu et al., 1995, 2000). Furthermore, astrocytes prevent neurite extension beyond the “walls” of the barrels in somatosensory cortex (Steindler et al., 1995). In addition, astrocytes play a prominent role in creating an environment that is nonpermissive to axonal growth in lesions (Stichel and Müller, 1998), while in a complementary fashion cortical or striatal astrocytes attract more axons in a neural co-graft than ventral mesencephalic astrocytes (Petit et al., 2001).

The heterogeneity among astroglia reported here suggests that specific combinations of diverse populations establish migration limits, not only as a physical impediment but also by determining the environment permissiveness. For example, less permissive astroglia outside of the RMS may prevent cells from escaping the pathway rich in permissive astroglia. Moreover, OB-astroglia strongly enhances migration which may help to explain cell-detachment and radial migration from the RMS into the OB. Although several molecular factors influence this process (Hack et al., 2002; Ng et al., 2005; Saghatelyan et al., 2004), their cellular source is not clear. Interestingly, radial migration into the OB *in vivo* is faster than tangential migration along the RMS (Bovetti et al., 2007a). Thus, a more permissive astroglia population may facilitate migration, especially in the OB where neuroblasts now migrate in isolation rather than as chains which requires establishing contacts with other cellular substrates. Indeed, neuroblasts in the OB are closely associated with astrocyte processes that are apposed to blood vessels that may also contribute to the migratory scaffold (Bovetti et al., 2007b). Cell detachment from the RMS chains could be an integrating phenomenon that involves both molecular chemoattractants and a permissive astroglial population that would enhance migration.

Neurons Display Different Migratory Behavior Depending on the Astrocyte Origin

Time-lapse analyses showed neuroblasts migrate faster and have shorter stationary periods on OB-astrocytes relative to those on Cx-astrocytes. Our estimates of velocity are consistent with *in vivo* data (Nam et al., 2007). Furthermore, neuroblast stationary periods were augmented on RMS- and Cx-astrocytes, producing a reduction in the average distance from the origin. This could be related to the cell speed decrease in the RMS (Fig. 1C in Bovetti et al., 2007a), or the numerous stops in the more rostral RMS (Nam et al., 2007), suggesting that migration in RMS is limited by astrocyte-derived-factors. In addition, both *in vivo* (Nam et al., 2007) and *in vitro* data (see results, Fig. 4D–F) show that RMS is composed of different motile cell classes defined by their trajectories and speed; intragroup variability could mask significant differences for other parameters in time-lapse analyses.

Nonsoluble Factors Associated with Astrocytes are Sufficient to Account for the Differences in RMS Cell Migration

RMS migration is influenced by different soluble and cell-contact molecules (for review Lledo et al., 2006; Menezes et al., 2002). However, our collagen assays failed to identify soluble glial-derived factors that enhance cell migration, as reported in Matrigel or poly-D-lysine rat cultures (Mason et al., 2001). Additionally, our data showed that nonsoluble astrocyte-bound-factors are directly responsible for differences in migration. Accordingly,

our data lead to the conclusion that astrocytes can enhance migration through cell–cell contact (Lim et al., 1999). Thus, we examined the expression of ECM and cell-adhesion related-genes. By analyzing different astroglial populations, this novel approach revealed new and significant differences among these populations not described in earlier studies (Cahoy et al., 2008). Of importance, most genes that differed significantly in RMS- and OB-astrocytes when compared with Cx-astrocytes were upregulated suggesting a proactive effect.

Diverse factors upregulated in the permissive monolayers were specifically related to RMS migration *in vivo*. Thus, laminins (Belvindrah et al., 2007; Murase and Horwitz, 2002), integrins (Belvindrah et al., 2007), and metalloproteases (Bovetti et al., 2007a) are decisive in this migration. Collagens in the RMS (Eagleson et al., 1996), are also implicated as scaffolding and regulatory elements. In addition, other proteins including *Sparc*, expressed in RMS (Vincent et al., 2008), or cadherin/catenin system proteins, implicated in chain migration (Taniguchi et al., 2006), may influence RMS migration. Lack of *Thbs1* leads to a widening of the RMS and consequently allows fewer neuronal precursors to reach the OB (Blake et al., 2008). This is even more evident in light of our data, which shows the importance of *Thbs1, Ecm1, Lama3, and Ctnna1* as potential mediators in postnatal migratory behavior. Thus, our data suggest that permissive astrocytes could generate a more favorable environment for migration through the upregulation of some specific genes. However, lower migration rates of neuroblast from the RMS explants on nonpermisive astrocyte monolayers, could also be related to inhibitory properties of astrocytes for cell migration. In fact, the presence of inhibitory factors such as chondroitinsulfate proteoglycans surrounding the SVZ/RMS, i.e. NG2-expressing cells, might be preventing neuroblasts from dispersing into the parenchyma (Komitova et al., 2009).

Exceptional Heterogeneity Between Close Astroglia Populations

Differences in permissiveness and gene expression highlight the heterogeneity between astroglial populations, as described in other brain areas, as seems to be common in the brain (Johnstone et al., 1986; Pindzola et al., 1993; Song et al., 2002). As we showed *in vitro*, heterogeneity is also conserved among neighboring populations *in vivo* (Garcia-Abreu et al., 1995). Thus, RMS-astrocytes have specific expression patterns (Peretto et al., 1997; Yamashita et al., 1997) and different proliferation rates (Emsley and Macklis, 2006).

While RMS- and OB-derived-astroglia display a bipolar morphology *in vitro*, Cx-derived-astrocytes are flat and extended. These differences reflect a similar morphology *in vivo*. Indeed, elongated astrocytes are observed in OB (Chiu and Greer, 1996) and SVZ/RMS (Garcia et al., 2004; Liu et al., 2006; Supp. Info. Fig. 1) while Cx-astrocytes are velated and protoplasmic (Emsley and Macklis, 2006). Since migration is greater on elongated astrocytes, morphology and permissiveness appear correlated. Similarly, differences in neuronal growth have been associated with different astrocyte morphologies (Meiners et al., 1995). However, an immature state was suggested for RMS-astrocytes *in vivo* (Liu et al., 2006; Peretto et al., 1997) and may be a co-variable in this correlation.

In summary, our data suggest that astroglia define the migration pathway, not simply as a cellular physical scaffold but rather by providing a molecular scaffold interposed between astrocytes and neuroblasts. The differences between the monolayers studied here raise the question as to how this heterogeneity is generated (if it is linked to spatio-temporal patterning during development) or maintained (factors such as neuronal activity or migration could be decisive). The answer to such questions could also shed light on how pathway restriction and detachment are determined.

Supplementary Material

Refer to Web version on PubMed Central for supplementary material.

Acknowledgments

The authors thank Alfonso Araque, Albert Blanchart, and Fernando García-Moreno for helpful comments on the manuscript. They also thank Dolores Montoya and Wolfang Pita for their technical assistance.

Grant sponsor: MICINN; Grant number: BFU2007-60351/BFI; Grant sponsor: OLFACTOSENSE Consortium (CAM); Grant number: P-SEM-0255-2006; Grant sponsor: Castilla-La Mancha Health Research Foundation; Grant number: FISCAM PI2007-66.

REFERENCES

Alves JA, Barone P, Engelender S, Froes MM, Menezes JR. Initial stages of radial glia astrocytic transformation in the early postnatal anterior subventricular zone. J Neurobiol. 2002; 52:251–265. [PubMed: 12210108]

Banker, G.; Goslin, K., editors. Culturing nerve cells. Cambridge: MIT Press; 1991. p. 453

Belvindrah R, Hankel S, Walker J, Patton BL, Muller U. Beta1 integrins control the formation of cell chains in the adult rostral migratory stream. J Neurosci. 2007; 27:2704–2717. [PubMed: 17344408]

Blake SM, Strasser V, Andrade N, Duit S, Hofbauer R, Schneider WJ, Nimpf J. Thrombospondin-1 binds to ApoER2 and VLDL receptor and functions in postnatal neuronal migration. Embo J. 2008; 27:3069–3080. [PubMed: 18946489]

Bolteus AJ, Bordey A. GABA release and uptake regulate neuronal precursor migration in the postnatal subventricular zone. J Neurosci. 2004; 24:7623–7631. [PubMed: 15342728]

Bovetti S, Bovolin P, Perroteau I, Puche AC. Subventricular zone-derived neuroblast migration to the olfactory bulb is modulated by matrix remodelling. Eur J Neurosci. 2007a; 25:2021–2033. [PubMed: 17439490]

Bovetti S, Hsieh YC, Bovolin P, Perroteau I, Kazunori T, Puche AC. Blood vessels form a scaffold for neuroblast migration in the adult olfactory bulb. J Neurosci. 2007b; 27:5976–5980. [PubMed: 17537968]

Cahoy JD, Emery B, Kaushal A, Foo LC, Zamanian JL, Christopherson KS, Xing Y, Lubischer JL, Krieg PA, Krupenko SA, Thompson WJ, Barres BA. A transcriptome database for astrocytes, neurons, and oligodendrocytes: A new resource for understanding brain development and function. J Neurosci. 2008; 28:264–278. [PubMed: 18171944]

Chiu K, Greer CA. Immunocytochemical analyses of astrocyte development in the olfactory bulb. Brain Res Dev Brain Res. 1996; 95:28–37.

Doetsch F, Garcia-Verdugo JM, Alvarez-Buylla A. Cellular composition and three-dimensional organization of the subventricular germinal zone in the adult mammalian brain. J Neurosci. 1997; 17:5046–5061. [PubMed: 9185542]

Eagleson KL, Ferri RT, Levitt P. Complementary distribution of collagen type, IV the epidermal growth factor receptor in the rat embryonic telencephalon. Cereb Cortex. 1996; 6:540–549. [PubMed: 8670680]

Emsley JG, Macklis JD. Astroglial heterogeneity closely reflects the neuronal-defined anatomy of the adult murine CNS. Neuron Glia Biol. 2006; 2:175–186. [PubMed: 17356684]

Faiz M, Acarin L, Villapol S, Schulz S, Castellano B, Gonzalez B. Substantial migration of SVZ cells to the cortex results in the generation of new neurons in the excitotoxically damaged immature rat brain. Mol Cell Neurosci. 2008; 38:170–182. [PubMed: 18434192]

Garcia AD, Doan NB, Imura T, Bush TG, Sofroniew MV. GFAPexpressing progenitors are the principal source of constitutive neurogenesis in adult mouse forebrain. Nat Neurosci. 2004; 7:1233–1241. [PubMed: 15494728]

Garcia-Abreu J, Moura Neto V, Carvalho SL, Cavalcante LA. Regionally specific properties of midbrain glia: I Interactions with midbrain neurons. J Neurosci Res. 1995; 40:471–477. [PubMed: 7616607]

Garcia-Abreu J, Mendes FA, Onofre GR, De Freitas MS, Silva LC, Moura Neto V, Cavalcante LA. Contribution of heparan sulfate to the non-permissive role of the midline glia to the growth of midbrain neurites. Glia. 2000; 29:260–272. [PubMed: 10642752]

Hack I, Bancila M, Loulier K, Carroll P, Cremer H. Reelin is a detachment signal in tangential chain-migration during postnatal neurogenesis. Nat Neurosci. 2002; 5:939–945. [PubMed: 12244323]

Jankovski A, Sotelo C. Subventricular zone-olfactory bulb migratory pathway in the adult mouse: Cellular composition and specificity as determined by heterochronic and heterotopic transplantation. J Comp Neurol. 1996; 371:376–396. [PubMed: 8842894]

Johnstone SR, Levi G, Wilkin GP, Schneider A, Ciotti MT. Subpopulations of rat cerebellar astrocytes in primary culture: Morphology, cell surface antigens and [3H]GABA transport. Brain Res. 1986; 389:63–75. [PubMed: 2418929]

Kleinman HK, Martin GR. Matrigel: Basement membrane matrix with biological activity. Semin Cancer Biol. 2005; 15:378–386. [PubMed: 15975825]

Komitova M, Zhu X, Serwanski DR, Nishiyama A. NG2 cells are distinct from neurogenic cells in the postnatal mouse subventricular zone. J Comp Neurol. 2009; 512:702–716. [PubMed: 19058188]

Law AK, Pencea V, Buck CR, Luskin MB. Neurogenesis and neuronal migration in the neonatal rat forebrain anterior subventricular zone do not require GFAP-positive astrocytes. Dev Biol. 1999; 216:622–634. [PubMed: 10642797]

Lim DA, Alvarez-Buylla A. Interaction between astrocytes and adult subventricular zone precursors stimulates neurogenesis. Proc Natl Acad Sci USA. 1999; 96:7526–7531. [PubMed: 10377448]

Liu X, Bolteus AJ, Balkin DM, Henschel O, Bordey A. GFAPexpressing cells in the postnatal subventricular zone display a unique glial phenotype intermediate between radial glia and astrocytes. Glia. 2006; 54:394–410. [PubMed: 16886203]

Lledo PM, Alonso M, Grubb MS. Adult neurogenesis and functional plasticity in neuronal circuits. Nat Rev Neurosci. 2006; 7:179–193. [PubMed: 16495940]

Lois C, Alvarez-Buylla A. Long-distance neuronal migration in the adult mammalian brain. Science. 1994; 264:1145–1148. [PubMed: 8178174]

Lois C, Garcia-Verdugo JM, Alvarez-Buylla A. Chain migration of neuronal precursors. Science. 1996; 271:978–981. [PubMed: 8584933]

Luzzati F, Peretto P, Aimar P, Ponti G, Fasolo A, Bonfanti L. Glia-independent chains of neuroblasts through the subcortical parenchyma of the adult rabbit brain. Proc Natl Acad Sci USA. 2003; 100:13036–13041. [PubMed: 14559968]

Mason HA, Ito S, Corfas G. Extracellular signals that regulate the tangential migration of olfactory bulb neuronal precursors: Inducers, inhibitors, and repellents. J Neurosci. 2001; 21:7654–7663. [PubMed: 11567055]

Meiners S, Powell EM, Geller HM. A distinct subset of tenascin/CS-6-PG-rich astrocytes restricts neuronal growth *in vitro*. J Neurosci. 1995; 15:8096–8108. [PubMed: 8613745]

Menezes JR, Marins M, Alves JA, Froes MM, Hedin-Pereira C. Cell migration in the postnatal subventricular zone. Braz J Med Biol Res. 2002; 35:1411–1421. [PubMed: 12436184]

Murase S, Horwitz AF. Deleted in colorectal carcinoma and differentially expressed integrins mediate the directional migration of neural precursors in the rostral migratory stream. J Neurosci. 2002; 22:3568–3579. [PubMed: 11978833]

Nam SC, Kim Y, Dryanovski D, Walker A, Goings G, Woolfrey K, Kang SS, Chu C, Chenn A, Erdelyi F, Szabo G, Hockberger P, Szele FG. Dynamic features of postnatal subventricular zone cell motility: A two-photon time-lapse study. J Comp Neurol. 2007; 505:190–208. [PubMed: 17853439]

Ng KL, Li JD, Cheng MY, Leslie FM, Lee AG, Zhou QY. Dependence of olfactory bulb neurogenesis on prokineticin 2 signaling. Science. 2005; 308:1923–1927. [PubMed: 15976302]

Noctor SC, Flint AC, Weissman TA, Dammerman RS, Kriegstein AR. Neurons derived from radial glial cells establish radial units in neocortex. Nature. 2001; 409:714–720. [PubMed: 11217860]

Pencea V, Luskin MB. Prenatal development of the rodent rostral migratory stream. J Comp Neurol. 2003; 463:402–418. [PubMed: 12836176]

Peretto P, Merighi A, Fasolo A, Bonfanti L. Glial tubes in the rostral migratory stream of the adult rat. Brain Res Bull. 1997; 42:9–21. [PubMed: 8978930]

Petit A, Pierret P, Vallee A, Doucet G. Astrocytes from cerebral cortex or striatum attract adult host serotoninergic axons into intrastriatal ventral mesencephalic co-grafts. J Neurosci. 2001; 21:7182–7193. [PubMed: 11549729]

Pindzola RR, Doller C, Silver J. Putative inhibitory extracellular matrix molecules at the dorsal root entry zone of the spinal cord during development and after root and sciatic nerve lesions. Dev Biol. 1993; 156:34–48. [PubMed: 7680631]

Platel JC, Dave KA, Bordey A. Control of neuroblast production and migration by converging GABA and glutamate signals in the postnatal forebrain. J Physiol. 2008; 586:3739–3743. [PubMed: 18467361]

Rydholm S, Rogers RA, Brismar H. Parafilm dependant cell patterning. Microsc Microanal. 2005; 11:1174–1175.

Saghatelyan A, de Chevigny A, Schachner M, Lledo PM. Tenascin- R mediates activity-dependent recruitment of neuroblasts in the adult mouse forebrain. Nat Neurosci. 2004; 7:347–356. [PubMed: 15034584]

Song H, Stevens CF, Gage FH. Astroglia induce neurogenesis from adult neural stem cells. Nature. 2002; 417:39–44. [PubMed: 11986659]

Steindler DA, Settles D, Erickson HP, Laywell ED, Yoshiki A, Faissner A, Kusakabe M. Tenascin knockout mice: Barrels, boundary molecules, and glial scars. J Neurosci. 1995; 15(3, Part 1): 1971–1983. [PubMed: 7534342]

Stichel CC, Muller HW. The CNS lesion scar: New vistas on an old regeneration barrier. Cell Tissue Res. 1998; 294:1–9. [PubMed: 9724451]

Suzuki SO, Goldman JE. Multiple cell populations in the early postnatal subventricular zone take distinct migratory pathways: A dynamic study of glial and neuronal progenitor migration. J Neurosci. 2003; 23:4240–4250. [PubMed: 12764112]

Taniguchi H, Kawauchi D, Nishida K, Murakami F. Classic cadherins regulate tangential migration of precerebellar neurons in the caudal hindbrain. Development. 2006; 133:1923–1931. [PubMed: 16611692]

Thomas LB, Gates MA, Steindler DA. Young neurons from the adult subependymal zone proliferate and migrate along an astrocyte, extracellular matrix-rich pathway. Glia. 1996; 17:1–14. [PubMed: 8723838]

Vincent AJ, Lau PW, Roskams AJ. SPARC is expressed by macroglia and microglia in the developing and mature nervous system. Dev Dyn. 2008; 237:1449–1462. [PubMed: 18366138]

Wang X, Seed B. A PCR primer bank for quantitative gene expression analysis. Nucleic Acids Res. 2003; 31:e154. [PubMed: 14654707]

Wichterle H, Garcia-Verdugo JM, Alvarez-Buylla A. Direct evidence for homotypic, glia-independent neuronal migration. Neuron. 1997; 18:779–791. [PubMed: 9182802]

Yamashita N, Kosaka K, Ilg EC, Schafer BW, Heizmann CW, Kosaka T. Selective association of S100A6 (calcyclin)-immunoreactive astrocytes with the tangential migration pathway of subventricular zone cells in the rat. Brain Res. 1997; 778:388–392. [PubMed: 9459556]

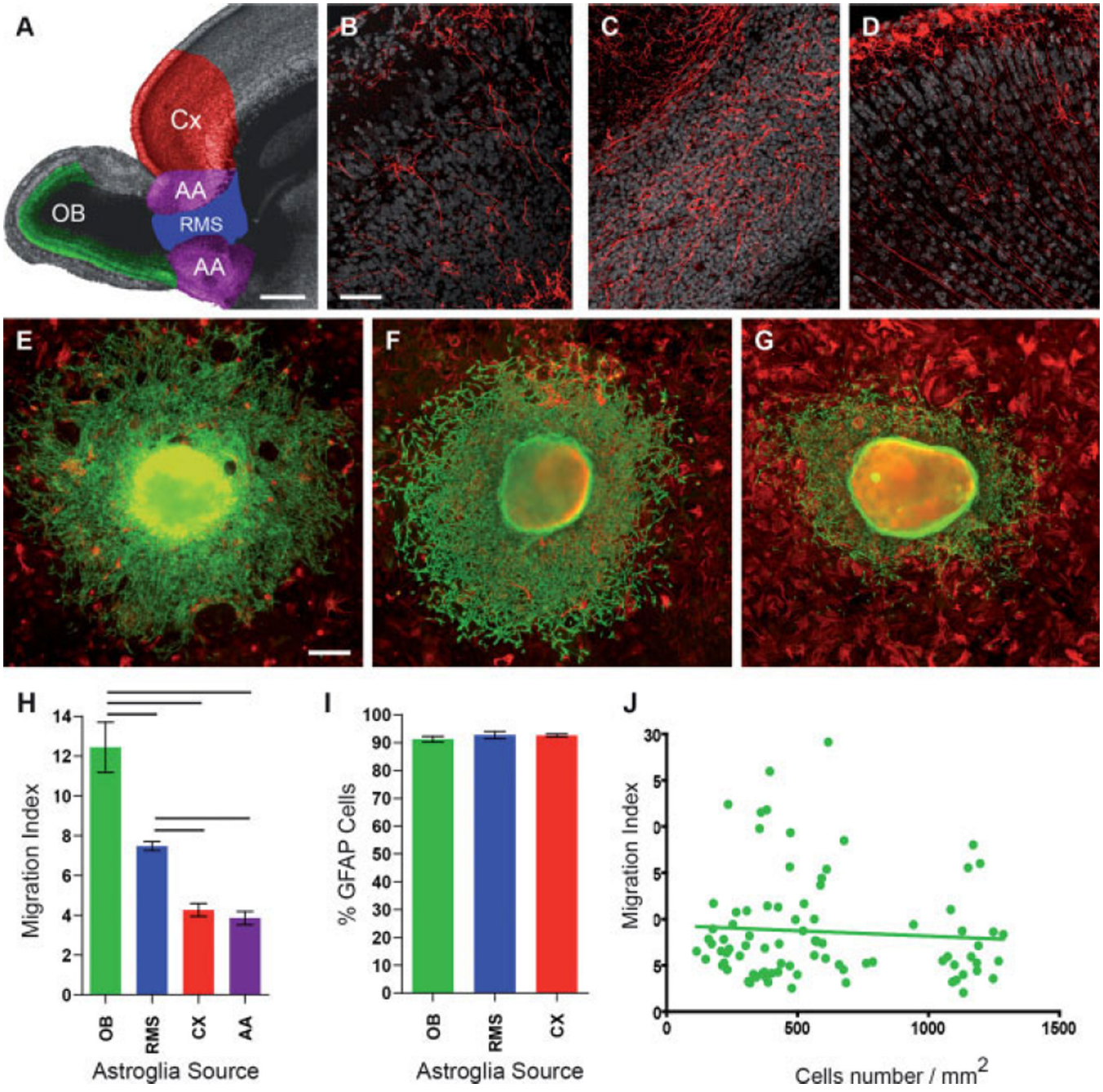

Fig. 1.

RMS-explants cultured on astrocyte monolayers derived from permissive (RMS, OB) and nonpermissive areas (frontal Cx and other adjacent RMS regions). (**A**) Shaded areas indicate the regions removed to generate the different astrocyte monolayers. (**B–D**) Immunohistochemistry for GFAP in sagittal sections at P2 (cell nuclei counterstained with bisbenzimide are shown in grey) from the OB (B), RMS (C) and CX (D). (**E–G**) Neuroblasts migrating from a RMS-explant (TuJ1, green) on astrocyte monolayers (GFAP, red) from OB (E), RMS (F) and Cx (G). (**H**) Neuroblast M.I. is statistically higher in those cells cultured on OB and RMS-derived-astrocytes than in those cultured on astrocytes from adjacent areas (where neuroblast migration does not occur *in vivo*). (**I**) Graph illustrates the

percentage of GFAP-positive cells in the astrocyte monolayers, showing a minimum of 91% astrocytes in the different monolayers. (**J**) Linear correlation analysis between cell density and M.I., showing no co-relation between both parameters. Horizontal lines between groups indicate significant differences. Error bars show SEM. Scale bar = 400 μm in A; 50 μm for B–D; 200 μm for E–G.

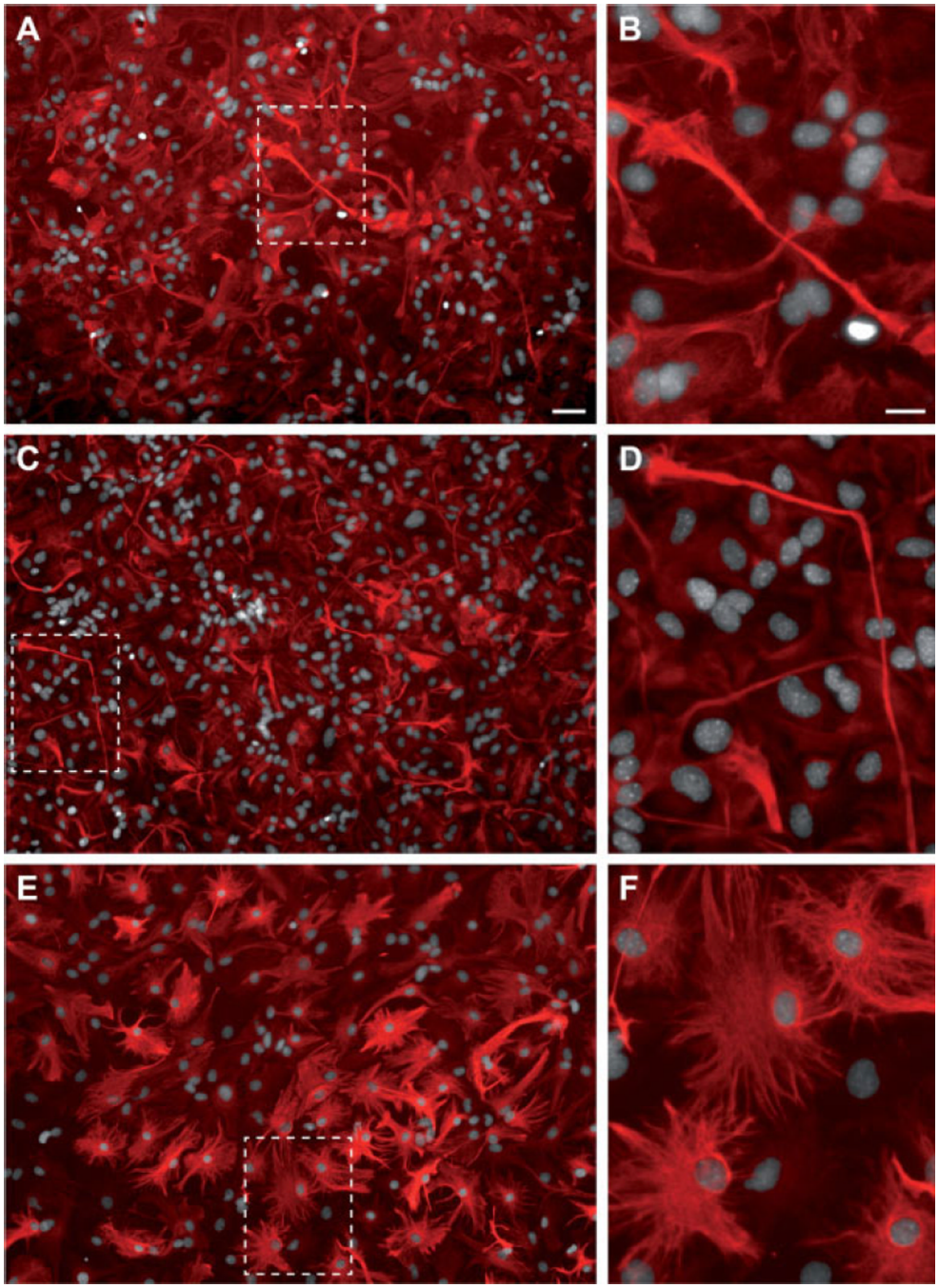

Fig. 2.

Morphologies of astrocytes from different origins immunostained with anti-GFAP. (**A,B**) OB. (**C,D**) RMS. (**E,F**) Cx. OB- and RMS-astrocytes show bipolar morphology while Cx-astrocytes have a stellate and flat morphology. Scale bar = 50 for A, C, E; 20 μm for B, D, F.

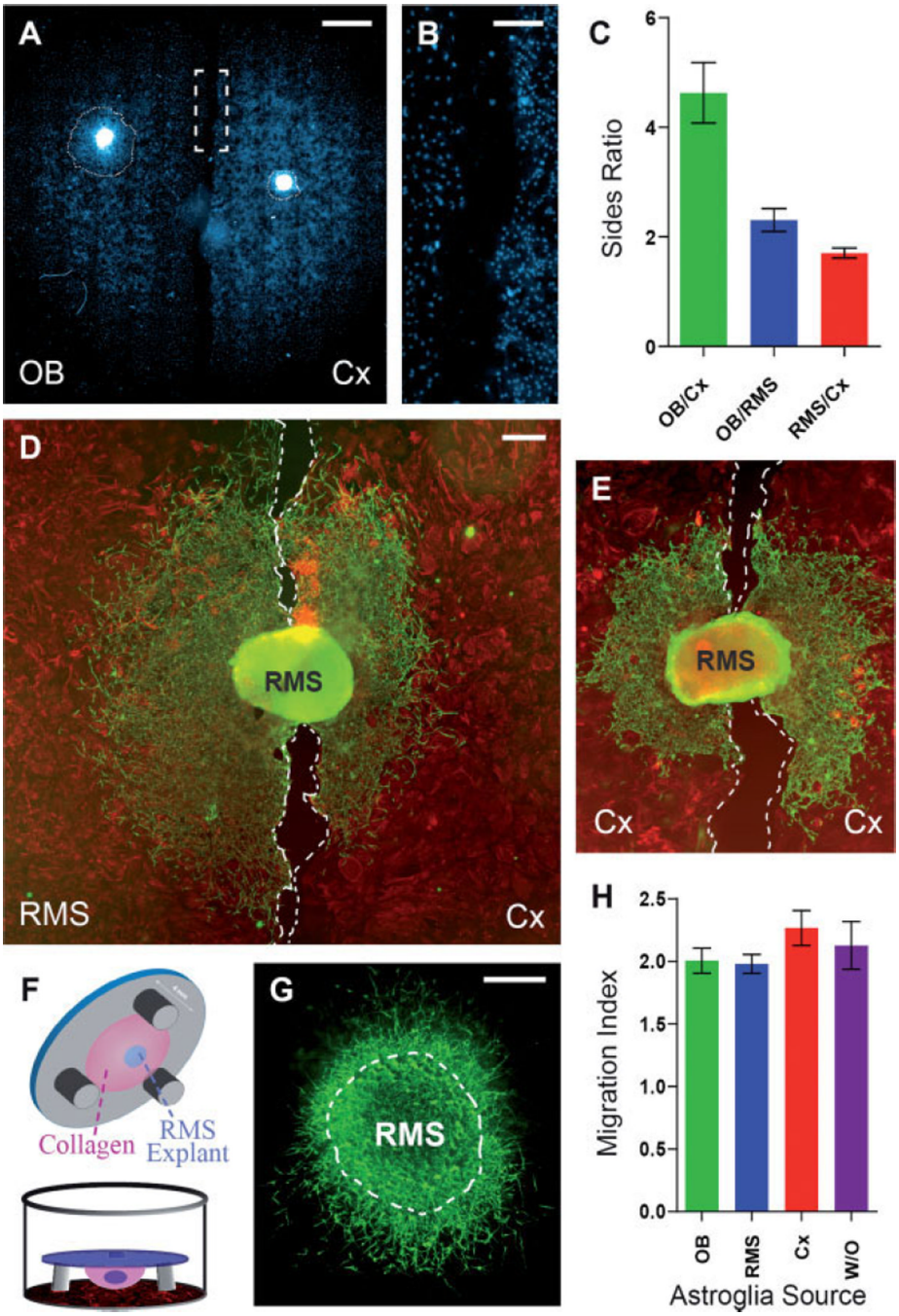

Fig. 3.

Differences in neuroblast migration on different astrocyte monolayers are not mediated by soluble factors. (**A**) Two-explants cultured on different astrocytes sources stained with bisbezimide. Dotted lines delimited the migration limits for each explant. (**B**) Dotted square in (A) shows the free cell line between the different astrocytes sources. (**C**) Graph corresponding to the neuroblast migration ratio between two RMS-explants plated on two different astrocyte monolayers in the same well. (**D**) RMS-explant cultured at the boundary between RMS and Cx-astrocytes stained for Tuj1 (green) and GFAP (red). Note the difference in migration is maintained even when the RMS-explant is positioned in between

different astrocyte monolayers. (**E**) RMS-explant plated in between two different Cx astrocyte monolayers. Note there are no significant differences in the migratory area. (**F**) Cartoon representing co-cultured RMS-explants on collagen over astrocyte monolayers. (**G**) RMS-explant co-cultured in collagen over astrocytes stained with anti-TuJ1. (**H**) Comparison of the migration index in the collagen co-culture on different astrocyte monolayers. W/O indicates assay without astrocytes. Error bars show SEM. Scale bar = 1.5 mm in A; 300 μm in B; 200 μm for D-E; 100 μm in G.

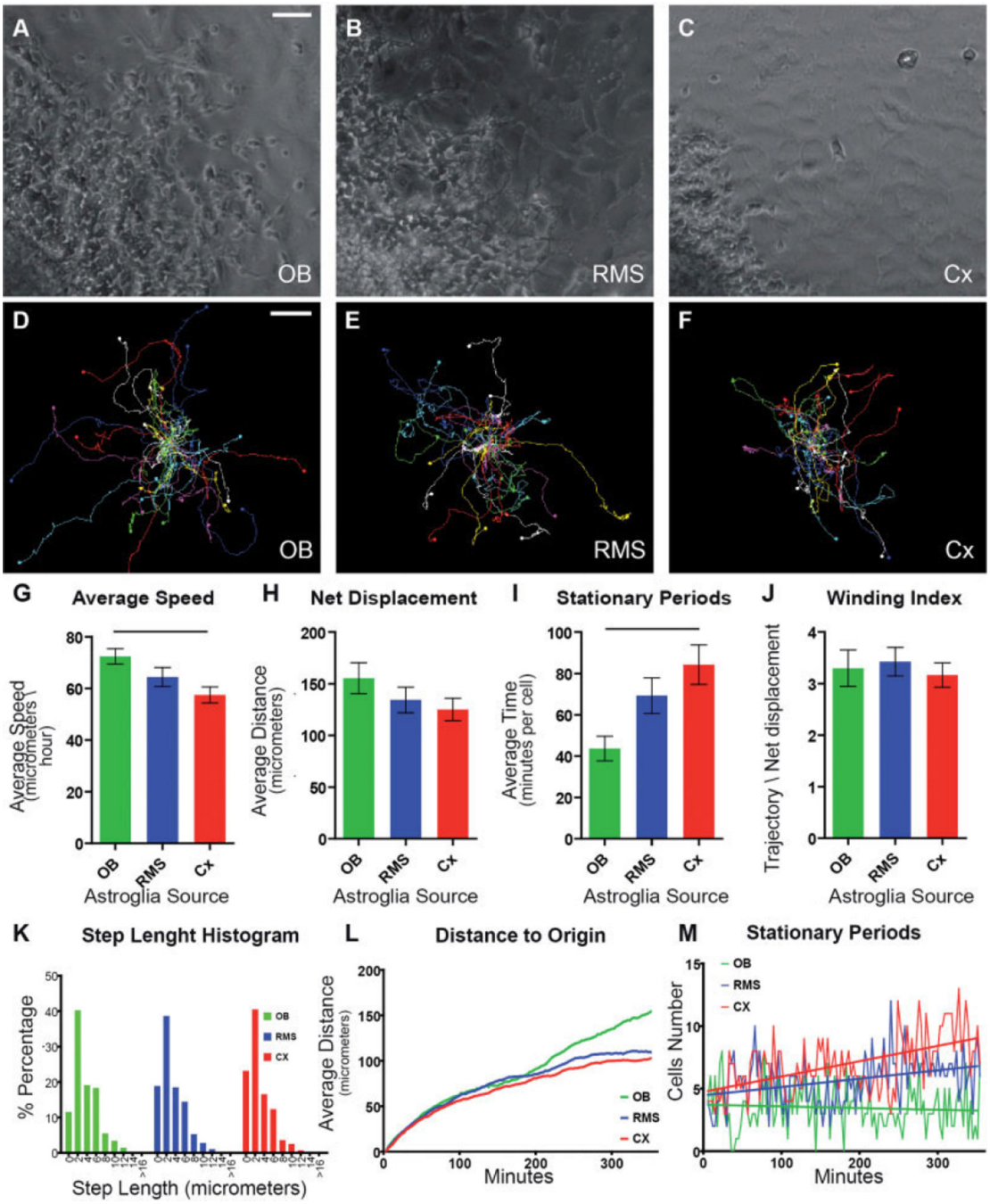

Fig. 4.

Time-lapse videomicroscopy of RMS-explants cultured on different astrocyte monolayers. (**A–C**) Neuroblast migration on astrocyte monolayers from OB (A), RMS (B) and Cx (C). The extension of cell migration is greater in OB- and RMS-derived astrocytes than on Cx-astrocytes. (**D–F**) Individual cell trajectories plotted over the last 6 h of the culture and adjusted to a common origin point. (**G**) Average speed of cell migration during the 6-h period. (**H**) Average of the maximum distance traveled away from the explant during the 6-h period. (**I**) Average of the cell stationary periods during the 6 h. (**J**) Average of the ratio between the total distance covered and the maximum distance reached from the migratory

origin. (**K**) Histogram of the step length shown in percentages. Each step is defined as 3-min period. (**L**) Graph showing the temporal average cell distance from the migration origin. (**M**) Graph represents the relationship between the number of paused cells and time. A linear regression analysis was used to evaluate the relationship between the number and the time of stopped cells. The slope was statistically non-zero for RMS and Cx-derived-astrocytes ($P < 0.0001$ in both cases), but not for OB-derived-astrocytes ($P = 0.424$). Horizontal lines between groups indicate significant differences. Error bars show SEM. Scale bar = 50 μm for A–C; 75 μm for D–F.

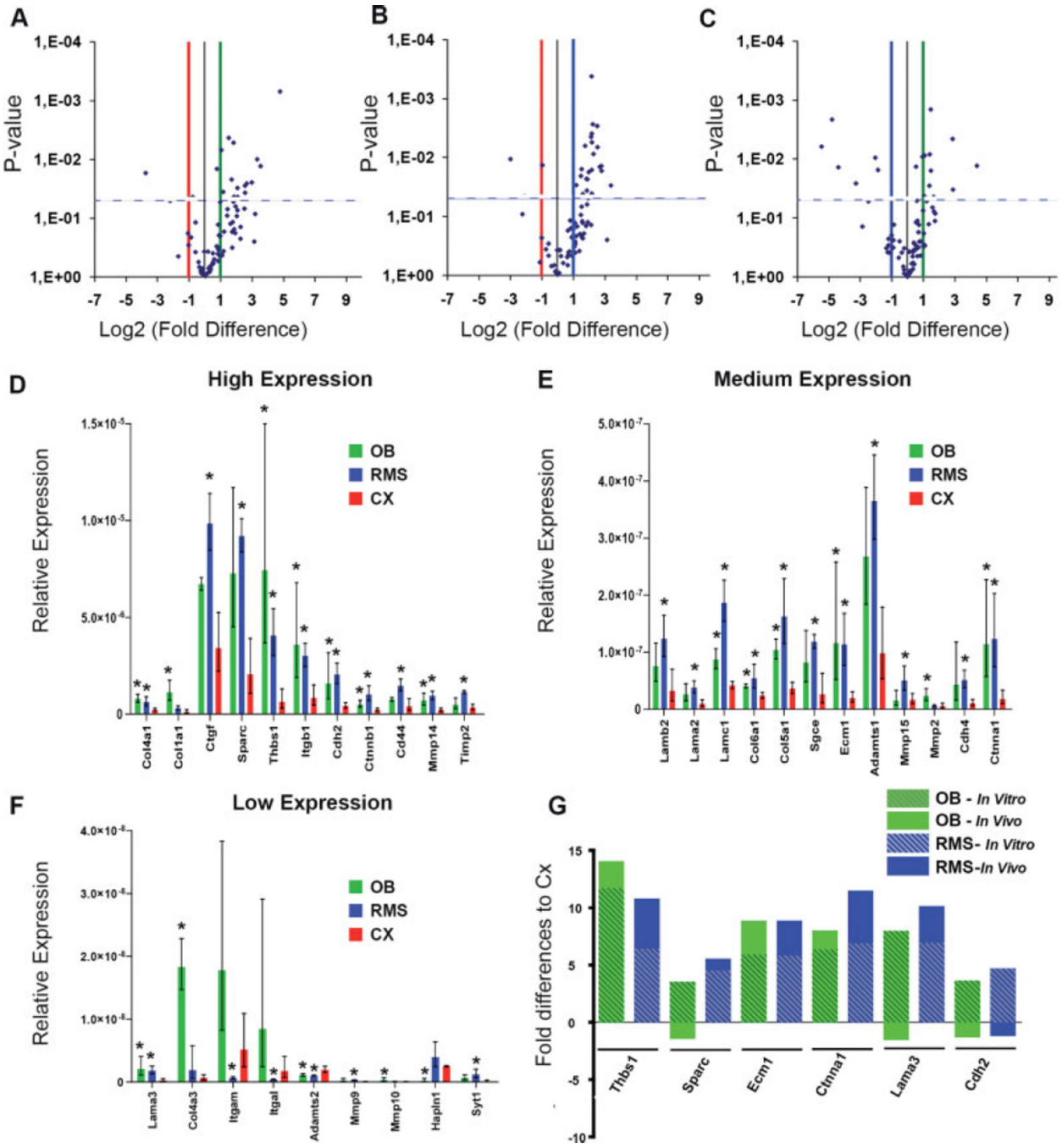

Fig. 5.

Comparative RT-PCR analysis of ECM and cell adhesion gene expression in the different astrocyte monolayers. (**A–C**) Graphs showing the *P*-value and the differences for each gene comparing OB vs. Cx-astrocytes (A), RMS vs. Cx-astrocytes (B) and RMS vs. OB-astrocytes (C). (**D–F**) Relative expression for high (D), medium (E) and low expressed (F) genes. (**G**) Correlated relative expression between *in vivo* and *in vitro* assays for some selected genes. Graph illustrates the differences in gene expression detected in cultured astrocytes from RMS, OB and Cx compared with freshly-dissected RMS, OB and Cx tissue

by RT-PCR. Asterisks indicate significant differences with respect to Cx-astrocytes. Bars show data range.